The physical meaning of time-delayed collection field transients from disordered devices

Markus Hußner ; Carsten Deibel ; Roderick C. I. MacKenzie ✉
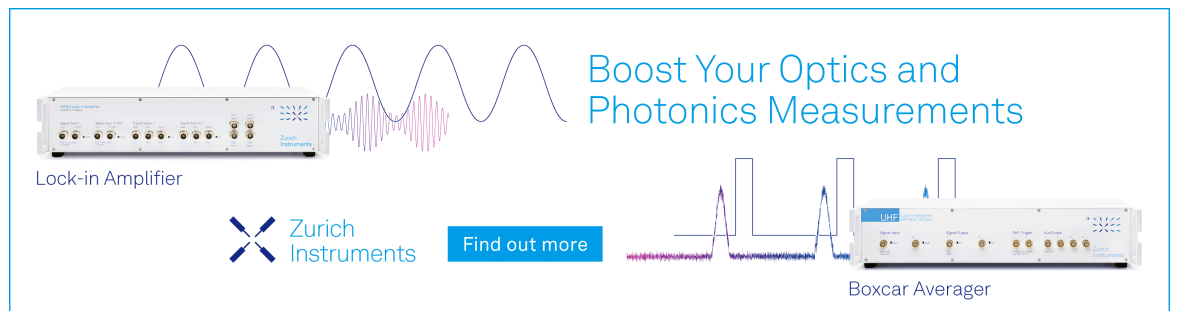
Check for updates

View Online

Export Citation

14 May 2024 14:17:29

The physical meaning of time-delayed collection field transients from disordered devices

Markus Hußner,[1] (ID) Carsten Deibel,[2,a)] (ID) and Roderick C. I. MacKenzie[1,b)] (ID)

AFFILIATIONS

[1]Department of Engineering, Durham University, Lower Mount Joy, South Road, Durham DH1 3LE, United Kingdom

[2]Institut für Physik, Technische Universität Chemnitz, Reichenhainer Straße 70, D-09126 Chemnitz, Germany

[a)]deibel@physik.tu-chemnitz.de

[b)]Author to whom correspondence should be addressed: roderick.mackenzie@durham.ac.uk

ABSTRACT

Charge carrier mobility and recombination determine the performance of many opto-electronic devices such as solar cells, sensors, and light-emitting diodes. Understanding how these parameters change as a function of material choice, charge carrier density, and device geometry is essential for developing the next generation of devices. The time-delayed collection field (TDCF) technique is becoming a widely used method to measure both recombination and carrier transport with values derived from this method being widely reported for many material systems. However, most novel materials are highly disordered with a high density of trap states and standard TDCF theory neglects the influence of these states. In this work, we examine how reliable TDCF can be as a measurement technique when the device contains significant energetic disorder. We identify regimes where the results can be relied upon and where the results should be taken with more caution. Finally, we provide simple and easy to use experimental tests to help the experimentalist decide whether the physical processes are dominated by trap states.

I. INTRODUCTION

Recently, much effort has been dedicated to developing electronic devices based on conducting polymers and small molecules. There are many classes of devices using these material systems that have already been demonstrated including, organic photovoltaic (OPV) devices,[1] organic light-emitting diodes (OLEDs),[2] and optical sensors.[3] The materials offer mechanical flexibility,[4] and the ability to absorb and emit light over a wide range of wavelengths.[5,6] Two key material parameters that determine device performance are charge carrier mobility and recombination rate. Charge carrier mobility describes how conductive the device is while the recombination rate determines how long carriers can survive in a device. For example, in a solar cell, one would ideally like to have a high charge carrier mobility and a low recombination rate to enable photogenerated carriers to exit the device before they recombine. For OLEDs, one would like a high carrier mobility to minimize joule heating and a low recombination rate in all parts of the device except the emissive layer to maximize photon generation. Thus, having an accurate measure of both charge carrier mobility and

recombination rate is essential if materials are to be compared and evaluated in the search for more efficient devices.

However, in materials with a high number of trap states a single value of mobility is hard to define.[5,7,8] In general, one may define an effective mobility as

$$\mu_{\text{eff}} = \frac{1}{d} \int_0^d \frac{\mu_{\text{free}} n_{\text{free}}(x)}{n_{\text{free}}(x) + n_{\text{trap}}(x)} \, dx, \tag{1}$$

where μ_{free} is the charge carrier mobility of completely free carriers, n_{free} is the density of completely free carriers, and n_{trap} is the density of trapped carriers.[9,10] Free carriers will reside above the mobility edge and have more energy than trapped carriers, which will generally reside in mid-gap states. The expression can be better understood if one looks at two extreme cases. If $n_{\text{trap}} = 0$ and there are no trapped carriers, the effective mobility will be equal to μ_{free}. If, on the other hand, $n_{\text{free}} = 0$, then all carriers will be trapped and μ_{eff} will be zero. Thus, one can see that the effective mobility of an organic device depends on how the carriers are distributed in energy space.

For a layer of organic semiconductor deposited on glass with no contacts that is kept in the dark, the carrier density will be low and carriers will mainly reside in deep states, resulting in a low mobility. If metallic contacts are added charges will flood into the semiconductor filling the trap states and through the Pauli-exclusion principle, there will be more free carriers. If the sample is then illuminated, the carrier density will further increase, and because many of the trap states are already filled, the free states will become more populated again increasing the average charge carrier mobility. Applying a positive voltage will cause carriers to flood into the device and through the same reasoning increase the carrier density and, thus, mobility. Inversely, applying a negative voltage will drag carriers out of the device and lower the mobility. Consequently, it can be seen that mobility is very much dependent upon the exact conditions under which it is measured, and it cannot be assigned a single value in disordered materials. In much the same way, recombination is also highly carrier density dependent.

The TDCF method[11–13] is often used to determine charge carrier mobility and recombination in disordered materials. The method is depicted at the top of Fig. 1. The sample is held at a constant (usually positive) pre-bias V_{pre}, a short laser pulse is then applied, and after the delay time t_d, a large negative voltage V_{col} is
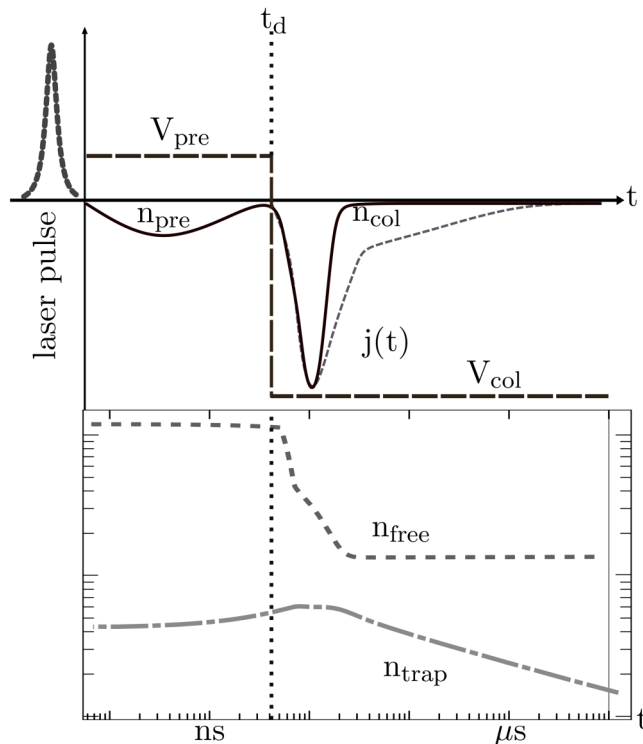
FIG. 1. Top: schematic diagram of a TDCF experiment. The solid and dashed lines labeled $j(t)$ represent the current measured for a material system with symmetric and very asymmetric mobilities in the presence of trap states. Bottom: the corresponding densities of free charge carriers n_{free} and trapped charge carriers n_{trap} for symmetric mobilities.

applied to extract photogenerated charge carriers that have not recombined. By studying how the total extracted charge changes as a function of t_d one can obtain recombination rates and by examining the gradient of the current transient, one can measure the charge carrier mobility.

However, if one considers the description of the TDCF method in combination with the discussion above about effective carrier mobility, it can immediately be seen that as soon as the TDCF voltage pulse is applied, it will start extracting carriers and, thus, change the mobility/energetic distribution of carriers within the device. As charge trapping is not considered in TDCF theory when attempting to recover mobility,[14] it is not clear what value of mobility will be extracted. Furthermore, this changing mobility would be expected to influence the charge extraction efficiency of TDCF and, therefore, change the measured recombination rate. Therefore, in this work, we examine the validity of TDCF to measure mobility and recombination.

II. METHODS

A. The model

The TDCF method can be used to investigate a wide range of opto-electronic devices. However, in this work, we focus on organic solar cells due to the prominence of the technique in the field. We study a state-of-the-art glass/ITO/SnO$_2$/PM6:Y6/MoO$_3$/Ag device structure[15] with an active layer thickness of 100 nm. We chose a PM6:Y6 device because with the emergence of small molecule acceptors, PM6:Y6 is quickly becoming a key model material system.[16] Simulated device parameters are set close to previously reported experimental values;[15] however, they are made symmetric where necessary to simplify understanding (see the supplementary material).

The numerical model used for the simulations (OghmaNano) is described in detail elsewhere.[17–19] However, in summary, the electric field profile within the device is calculated using Poisson's equation in one dimension. The movement of free charge carriers is described by solving the bi-polar drift-diffusion equations. Conservation of particles is forced using the carrier conservation equations. As discussed in Sec. I, it is important to consider charge carrier trapping in disordered devices. Indeed, it should be noted that standard drift-diffusion models, which do not consider trap states, are not valid for disordered systems as they will fail to reproduce the correct dependence of mobility and recombination rate as a function of voltage/carrier density. We, therefore, describe the trap states below the LUMO and above the HOMO mobility edges as two exponential distributions of states,

$$\rho^{e/h}(E) = N^{e/h} \exp\left(-\frac{E}{E_U^{e/h}}\right), \quad (2)$$

where $N^{e/h}$ are the electron/hole trap densities at the LUMO and HOMO edge; $E_U^{e/h}$ are the characteristic electron/hole tail slope energies; and E is the energy relative to the LUMO/HOMO edge. This distribution is then broken up into eight independent trap states of 0.1 eV in height, and the full time domain Shockley–Read–Hall[20] (SRH) equations are solved for each energetic range.
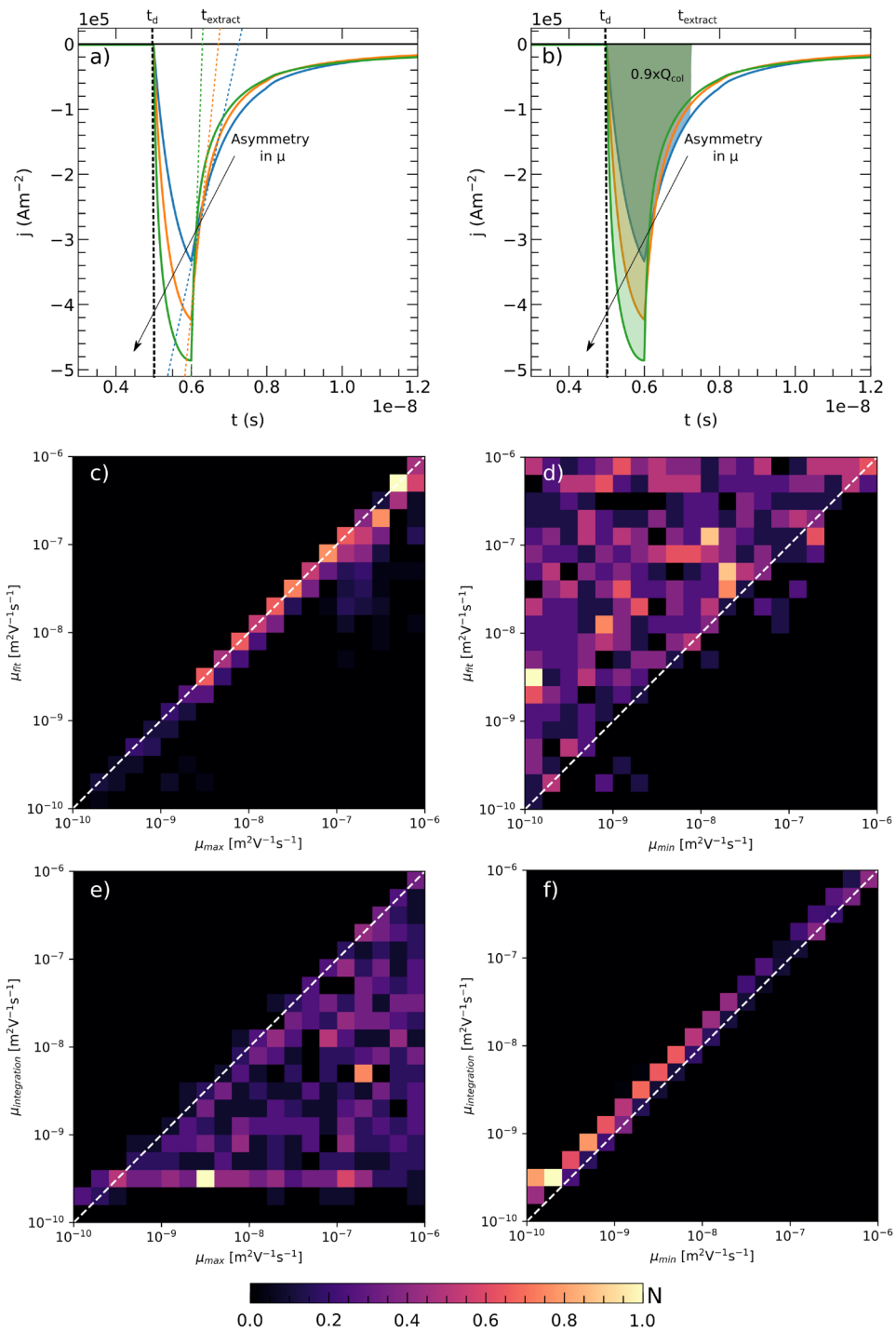
FIG. 2. (a) Fitting the initial linear photo-current decay to determine the mobility of the fastest charge carrier. (b) Integrating the phototransient to a time when 90% of the total charge carriers has been extracted as a way to determine the mobility of the slowest carrier. (c) and (e) The error matrices for asymmetric input mobilities when trying to determine μ_{min}, μ_{max} using the fitting method. The fitting method can determine the mobility of the fastest charge carrier. (d) and (f) The error matrices for asymmetric input mobilities when trying to determine μ_{min}, μ_{max} using the integration method can determine the mobility of the slowest charge carrier. Electron and hole mobilities were both randomly varied.

14 May 2024 14:17:29

The LUMO electron SRH trapping equation is written as

$$\frac{\partial n_t}{\partial t} = r_{ec} - r_{ee} - r_{hc} + r_{he}, \qquad (3)$$

where r_{ec} and r_{ee} are the electron capture/escape rates, while r_{hc} and r_{he} are the hole capture/escape rates into the electron trap, which describes recombination. The rates are functions of carrier depth and free/trapped carrier density.[18] An analogous equation can be written for holes. Thus, using this approach, the carrier density can be described in both energy and position space across the device.

B. Mobility

Often in OPV material systems, the electron and hole mobilities are different by one or two orders of magnitude. Before looking at the influence of trap states, we first investigate how sensitive TDCF is to asymmetric carrier mobilities in a device with no traps. In TDCF experiments, charge carrier mobility is obtained by first fitting the linear photo-current decay with the equation,[21]

$$I(t) = \frac{Q_0}{t_{tr}}\left(1 - \frac{t}{t_{tr}} + \frac{2RC}{t_{tr}}\right), \qquad (4)$$
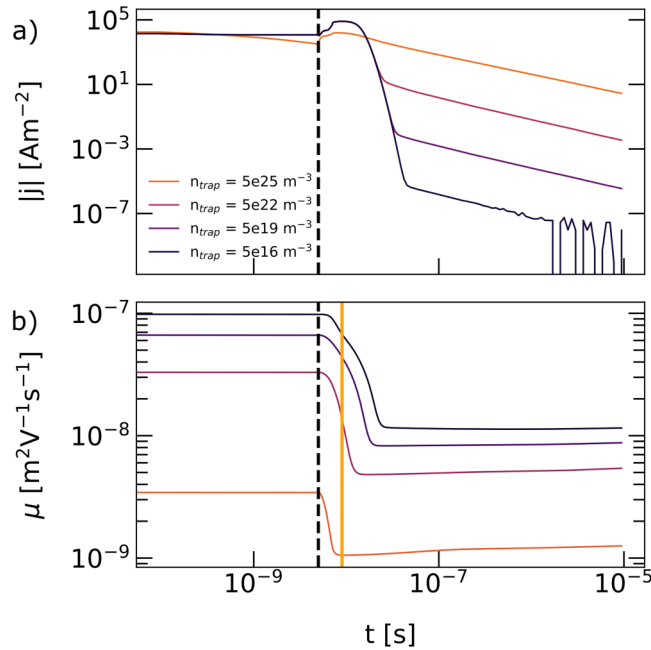
FIG. 3. (a) Comparison of current transients for different trap state densities and voltages. High trap state densities show a long lasting, high extraction current. (b) Effective mobility during the TDCF experiment. The vertical lines are guides to the eye. The black dashed line indicates the time at which extraction starts and the orange line represents the time at which the applied voltage has finished ramping to V_{col}.

to determine the extraction time t_{tr}, where Q_0 is the initial charge in the device before the decay. In this work, the $2RC/t_{tr}$ term is neglected as we only examine cases where the contribution is negligible, i.e., at least an order of magnitude less than the transit time. The charge carrier mobility μ is then calculated using

$$t_{tr} = \frac{d^2}{\mu V_0}, \qquad (5)$$

where d is the device thickness and V_0 is the applied voltage relative to the built-in potential. The blue line in Fig. 2(a) represents a TDCF transient where the device has symmetric electron/hole mobilities, while the orange and green lines represent the TDCF experiments with increasingly asymmetry in mobilities. Theoretically, fitting Eq. (4) to the linear decay will extract the mobility of the slower charge carrier species. However, in practice even for symmetric mobilities, it can be difficult to correctly determine the linear decay region because charge carrier diffusion and dispersion often broaden the transient. Furthermore, for asymmetric mobilities, current from both charge carriers can be present in the transient at the same time, making the fitting process more ambiguous.

Figure 2(c) plots the results of a series of simulations where a series of TDCF transients were simulated from devices with a range of electron and hole mobilities. The x axis plots the maximum of the electron/hole mobilities for the device $\max(\mu_e, \mu_h)$, while the y axis plots the mobility extracted using TDCF. It can be seen that TDCF can accurately extract the fastest mobility. Figure 2(e) plots the minimum value of device mobility $\min(\mu_e, \mu_h)$ plotted against the extracted TDCF mobility value. It can be seen that TDCF always overestimates the mobility of the slowest charge carrier. This is because the initial peak of current generated by the slower mobility carrier is always lower so in effect hidden by the larger current from the higher mobility carrier.

In an attempt to recover the mobility of the slowest charge carrier, we take inspiration from Lorrmann et al.[22] and numerically integrate the extraction current transient to the time when 90% of the total charge Q_{tot} is extracted to determine t_{tr}. Although the threshold is more or less arbitrary, by examining Fig. 2(d) and 2(f), one can see that the method can, indeed, extract the value of the slower charge carrier. It should, however, be pointed out that the effective and not free carrier mobility will be relevant for device operation.

Until now, we have considered a device without trap states where all carriers are free, $n_{trap} = 0$. However, in a realistic disordered device, n_{trap} will be typically be more than an order of magnitude higher than n_{free}. Furthermore, the values n_{free} to n_{trap} will change during a TDCF transient. This is depicted in the simulation at the bottom of Fig. 1. It can be seen that after the voltage pulse is applied, the number of free carriers rapidly drops as they are swept out the device and then much more gradually as the trapped carrier population decreases as thermal energy frees them, allowing them also to be swept out. This slow detrapping process has been previously described in Ref. 23.

Figure 3(a) depicts four TDCF transients with different densities of traps. A trap density of 5×10^{25} m^{-3} is considered very
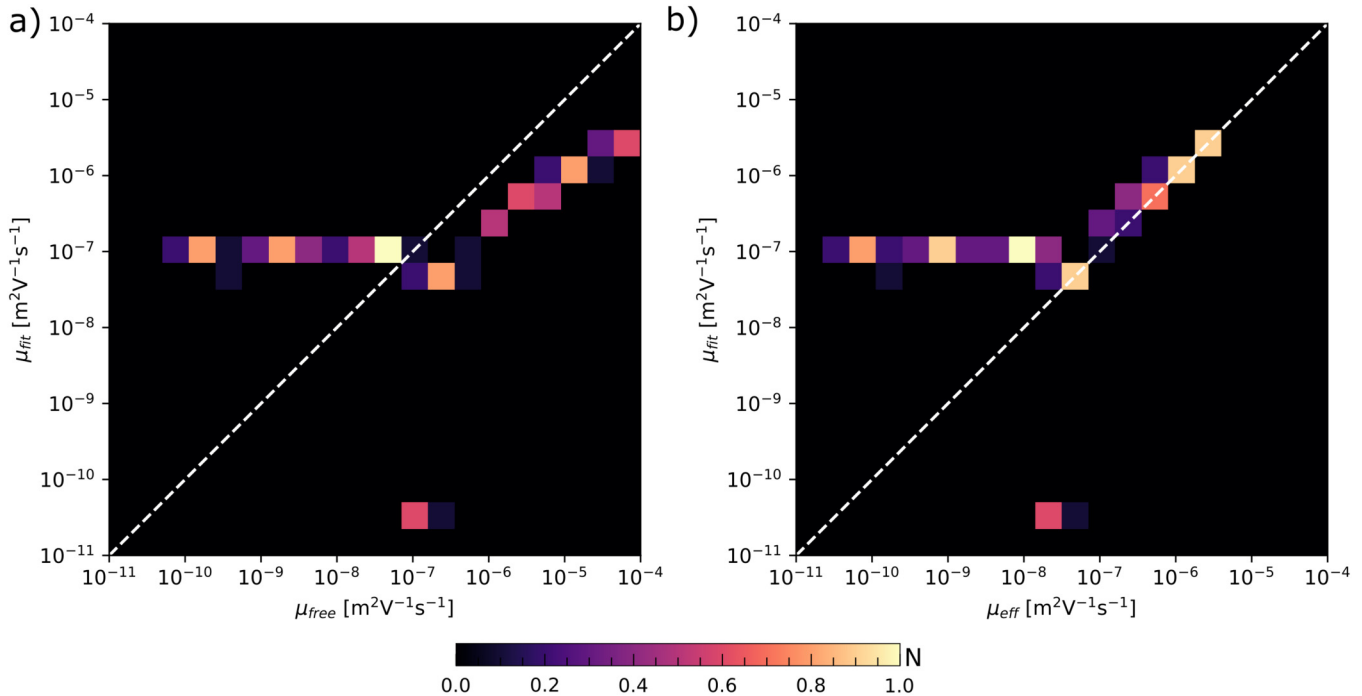
FIG. 4. (a) Comparison of free carrier mobility used to generate TDCF transients and the value of mobility extracted using the fitting method for a device with traps. (b) Comparison of effective carrier mobility just before the start of a TDCF transient plotted against the value of mobility extracted using the fitting method for a device with traps.

disordered, while a trap density of 5×10^{16} m^{-3} is considered quite trap free. It can be seen that for a device with many traps, the TDCF transient slowly drops off due to the long time it takes for trapped carriers to be extracted due to their slow release from the trap states. In contrast, a TDCF transient from a device with few trapped states rapidly drops off as there are no trap states preventing the extraction of carriers. Thus, a simple test to determine whether a device contains a significant number of trap states is to see if the TDCF transient decays rapidly or gradually.

The change in the effective mobility calculated using Eq. (1) is plotted in Fig. 3(b). It can be seen that due to the changing ratio of free to trapped carriers, the average mobility within the device changes during the transient. An interesting question to ask is which mobility do we extract with the TDCF method if the mobility is not constant? Do we measure the mobility at the start of the transient or the midpoint?

Figures 4(a) and 4(b) show the symmetric free carrier mobility and the effective mobility, respectively, used in the device model against that determined from the transient using the TDCF fitting method. As expected, TDCF does not extract accurate values of free carrier mobility: for high enough mobility values, we observe an underestimation of the effective carrier mobility by around half an order. This is because multiple trapping and release governs the charge transport. In general, it is worth noting that in an experiment such as TDCF where carriers are not hot, one will never be

able to extract the value of free carrier mobility. In contrast, the effective mobility—at least for values above 1×10^{-7} m^2 V^{-1} s^{-1}—can be reliably extracted from the TDCF data. Essentially, the effective mobility corresponds to the average mobility when considering that only the mobile charge carriers contribute to the current, not the trapped ones.

In summary, a high extraction current density at long times should be seen as a sign for a significant number of trap states. Nevertheless, for high enough effective charge carrier mobilities, TDCF is able to determine the values reliably. For lower mobilities, care should be taken when interpreting mobility values, and other techniques such as space-charge-limited current, frequency domain measurements, or simulations should be used to verify the results. Finally, we should conclude by noting that because charge carrier mobility is a strong function of carrier density; ideally, mobility should be measured as close to the operating point of a device as possible (i.e., P_{max} at one Sun for a solar cell) for the measurements to be most meaningful.

III. RECOMBINATION RATES

In general, there are two common pathways for recombination in solar cells. They are free-to-free recombination, which will have a recombination order of two, and free-to-trap recombination, which has a recombination order of one or larger. In disordered

14 May 2024 14:17:29
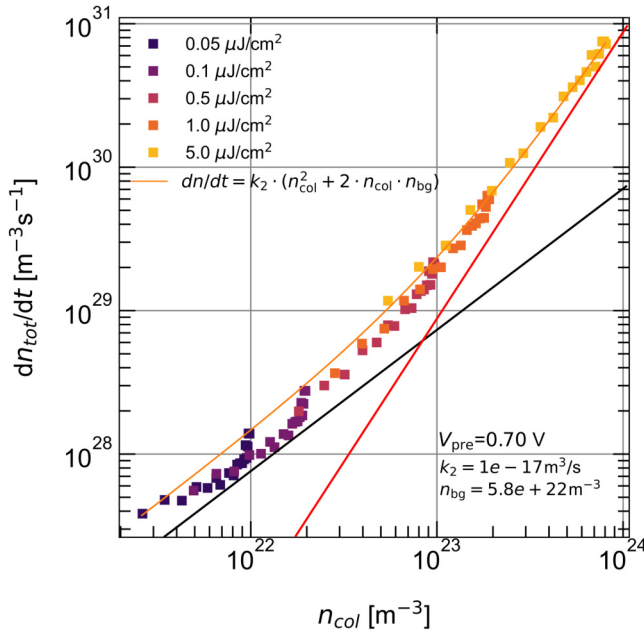
FIG. 5. Recombination rate from a nominally good reference PM6:Y6 device[25] plotted against collected carrier density. Solid lines are guides to the eye with the black line representing a slope of $\delta = 1$ and the red line representing a slope of $\delta = 2$. The orange line is a fit of Eq. (7) to the experimental data.

systems, there are many more trapped carriers than mobile carriers and, thus, the latter mechanism will usually dominate the bulk recombination rate. However, surface recombination at the contacts will push the recombination order toward one. Identifying the dominate recombination process can give important information on how to minimize losses in a device.[24]

Recombination can be probed with TDCF by varying the delay time t_d. The integrated photo-current is equal to the charge extracted from the device. By plotting the extracted charge carrier density n_{tot} with respect to the delay time, a recombination rate can be extracted. If the recombination rate is plotted over the collected charge carrier density n_{col} that survived recombination during the delay time, it is possible to extract the recombination order. The recombination order δ is extracted from the slope of the recombination rate,

$$\delta = \frac{d\{\log(R)\}}{d\{\log(n_{col})\}}, \quad (6)$$

in a log–log plot. For a given illumination intensity, recombination rates at high charge carrier densities correspond to small delay times.

To better understand the results produced by TDCF, we now apply the method to three distinctly different solar cells. First, we examine a well working PM6:Y6 solar cell based on previously published parameters;[25] then, we decrease the free-to-free recombination constant to investigate the case where recombination is dominated by contact recombination; and finally, we examine the case where recombination is dominated by trap assisted (SRH) processes. The exact parameters used can be found in the supplementary material.

Figure 5 plots simulated dn_{tot}/dt against n_{col} for a well working PM6:Y6 device.[25] Each color on the graph represents a different laser intensity, within each laser intensity, each point represents a single delay time. At low light intensities, surface recombination dominates as indicated by the recombination order of one (black solid line). For high illumination intensities, bi-molecular recombination with a recombination order of two dominates (red solid line).

By fitting the rate equation for bi-molecular, recombination[26,27]

$$\frac{dn}{dt} = k_2 \cdot \left(n_{col}^2 + n_{col}n_{bg}\right), \quad (7)$$

to the data in Fig. 5, we can extract the recombination constant k_2 and the background charge carrier density n_{bg}.

Figure 6(a) again plots dn_{tot}/dt against the collected charge, but this time for a device with a low value of free-to-free recombination. It can be seen that each colored data set consists of two distinct regions, a gradually rising region followed by an inflection point and then a very steep region. In our device without trap states, the very steep region probably implies surface recombination at the contacts.[25,28]

To verify that surface recombination was indeed the dominating process, we picked one illumination intensity from Fig. 6(a) ($I = 0.1 \ \mu J\,cm^{-2}$) and recorded the recombination rate R and the charge density n as a function of time during the TDCF transient. We repeated this for all the transients, which makes up the $I = 0.1 \ \mu J\,cm^{-2}$ data set. The result is plotted as multi-colored crosses in Fig. 6(b). The colors represent the delay time t_d. Thus, darker colors represent transients extracted at later times. Plotted on the same figure are red squares, these represent recombination rates directly extracted from the simulated TDCF transients, as one would do if performing the experiment for real.

This enables a direct comparison between the measured recombination rate through TDCF and the time resolved recombination rates inside the device. To be able to directly compare surface recombination to bulk recombination rates, we normalized the surface recombination as

$$R_{surf} = \frac{J_{surf}}{e \cdot L} \quad (8)$$

by accounting for the device thickness L.

It can be seen that the recombination rate within the device at the onset of the extraction exactly matches the surface recombination obtained from the TDCF transients.

Experimentally, surface recombination is detected by plotting the recombination orders at equal delay times for all the intensities. In practice, this is done by fitting a straight line to the points in Fig. 6(a), which have the same delay time. This will result in one point per light intensity being used for the fit each time. The results from doing this can be seen in Fig. 6(c); as the
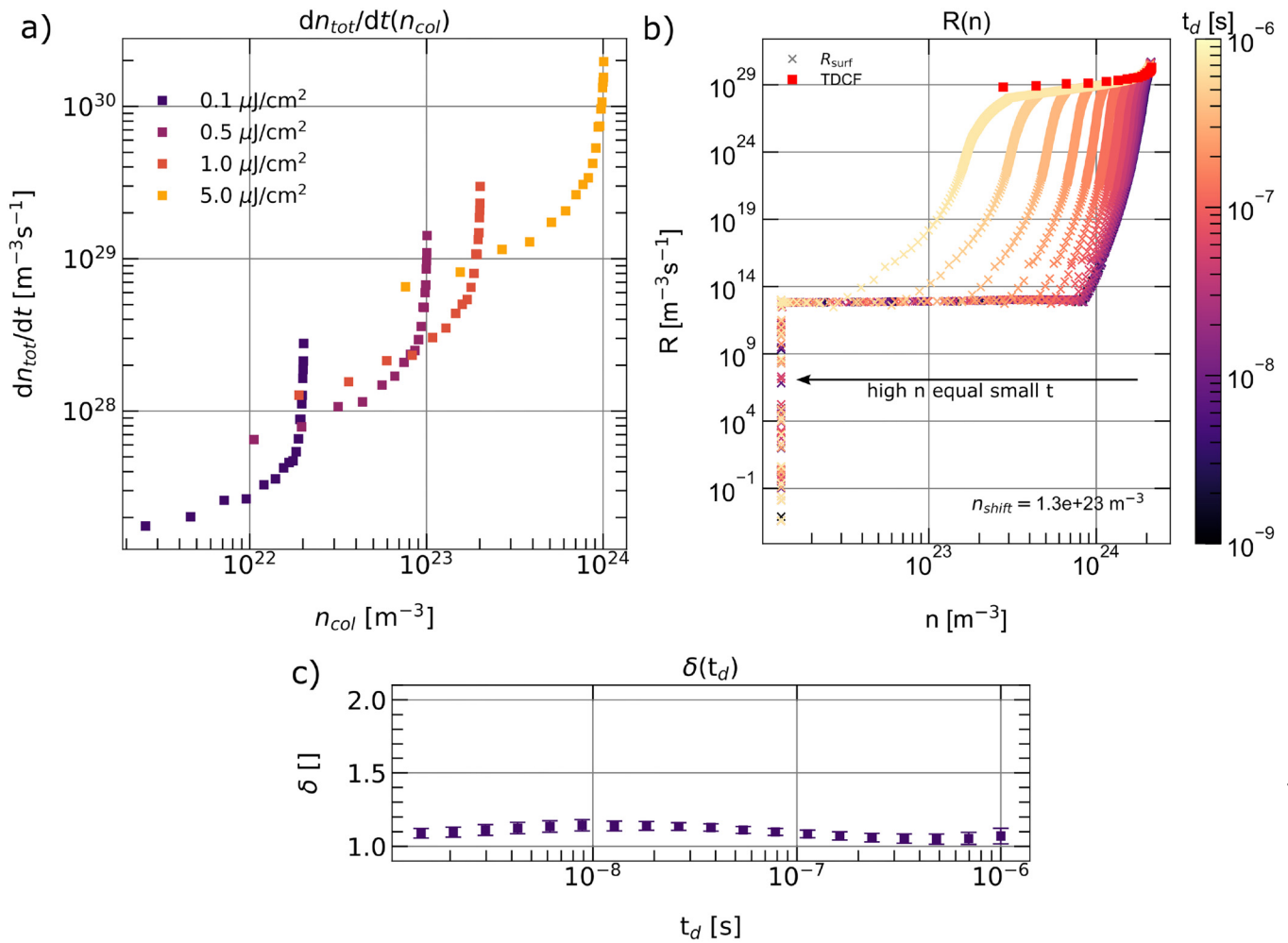
FIG. 6. A device where surface recombination dominates the TDCF transients due to no trap states and low free-to-free recombination rates. (a) Recombination rates extracted from simulated TDCF transients. (b) The recombination rate experienced by the device during charge carrier extraction for a range of delay times at a light intensity of $I = 0.1$ μJ cm^{-2}. (c) Time dependent recombination order $\delta(t_d)$ for the device, this is calculated by taking the gradient of (a) points collected at the same delay time.

recombination is of the order $\delta(t_d) = 1$, we can see that surface recombination is dominant in this device.

We now turn our attention to a device with energetic disorder. Figure 7(a) plots the recombination rates extracted from virtual TDCF transients from a device with a trap density of $N_{trap} = 10^{25}$ m^{-3}. For low light intensities, the curves look like the case where surface recombination dominates in that there is initially a gradual rise in the recombination rate followed by an inflection point.

Hofacker and Neher[29] show that the steep parts of the curves, which give high initial recombination orders in Fig. 7(a), are due to fast initial thermalization, which leads to rapidly dropping recombination rates, while the charge carrier density changes only a little. Once the initial thermalization is over, a quasi-equilibrium

establishes and an asymptotic value of the recombination order establishes. As optical excitation intensities increase, recombination rates become higher and dominate thermalization.

Figure 7(b) plots the recombination rates extracted from the TDCF transients at low light intensity $I = 0.1$ μJcm^{-2} as red squares. The crosses represent the R_{SRH}, which represents the loss of free carriers through SRH recombination and trapping. R_{SRH} was plotted within the TDCF transients for different delay times t_d. High values of carrier density represent early times, while low values of carrier density represent late times. It can be seen that the red squares sit to the very right-hand side of the graph. At this light intensity, we found R_{SRH} dominated by trapping rather than recombination. Thus, we concur with the results of Hofacker and Neher.[29]

14 May 2024 14:17:29
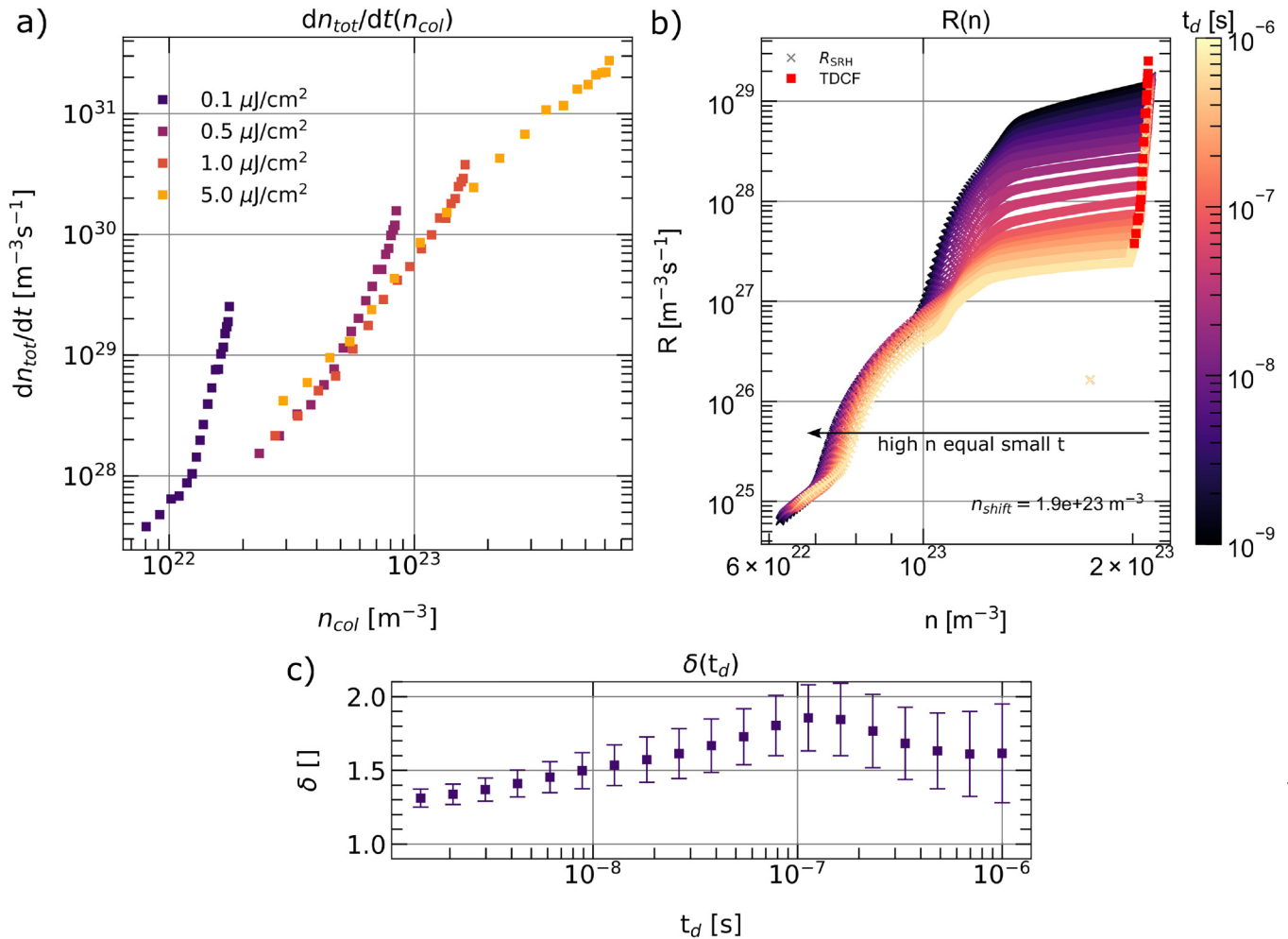
FIG. 7. A device where free-to-trap recombination dominates. (a) Recombination measured from virtual TDCF experiments for a device with traps $N_{trap} = 10^{25}$ m^{-3}. (b) Comparison of recombination rates extracted from TDCF experiments at $I = 0.1$ μJcm^{-2} plotted against the internal R_{SRH} recombination rate, which includes carrier trapping as well as recombination. (c) Extracted recombination order from (a).

Figure 7(c) plots the extracted recombination order from Fig. 7(a) as a function of delay time. A high initial recombination order with a time dependent recombination order $\delta \neq 1.0$ is an indicator for carrier thermalization and, therefore, an indication of trap states.

IV. CONCLUSION

The charge extraction technique TDCF is capable of extracting charge carrier mobility by analyzing the extraction current after applying a negative collection bias. The widely used method of fitting the initial photo-current decay (fit-method) is able to correctly determine the mobility of the faster charge carrier specimen in the case of negligible trap states and asymmetric charge carrier mobilities. To complement the fit-method, a second approach to detect the slower

charge carriers is proposed. By integrating the current transient to the time when 90% of charge carriers are extracted, t_d can be calculated and the mobility of the slower carrier to be determined. When trap states cannot be neglected, the TDCF method is able to determine effective mobility values reliably, if they are not too small. The current transient at early times is dominated by charge carrier relaxation into trap states. During the course of the extraction, a high number of charge carriers reside in trapped states.[23] These trapped carriers get freed step-by-step during the charge carrier extraction causing a long lasting high extraction current. The presence of the latter is an indicator of the presence of high trap state densities. The extracted mobilities might overestimate the effective mobilities and should be confirmed by other experimental methods or simulations.

By varying the delay time in TDCF, it is possible to probe the recombination in a device and extract the recombination order

14 May 2024 14:17:29

depending on charge carrier density. Recombination orders greater than 1 for small delay times can occur and are often explained with the presence of surface recombination. It is shown that this is true for cases with no or negligible trap states, but the thermalization of charge carriers in systems with high trap state densities can cause high initial recombination orders as well. Analyzing the time dependent recombination order can give information on the origin of the high initial recombination orders and is, therefore, the second indicator of non-negligible trap states in TDCF experiments. We conclude that TDCF is a powerful method. However, it should be applied with caution or the support of simulations.

SUPPLEMENTARY MATERIAL

Further example simulations can be found in the supplementary material.

AUTHOR DECLARATIONS

Conflict of Interest

The authors have no conflicts to disclose.

Author Contributions

Markus Hußner: Data curation (equal); Formal analysis (equal); Investigation (equal); Validation (equal); Visualization (equal); Writing – original draft (equal); Writing – review & editing (equal). **Carsten Deibel:** Investigation (equal); Methodology (equal); Supervision (equal); Writing – original draft (equal); Writing – review & editing (equal). **Roderick C. I. MacKenzie:** Investigation (equal); Methodology (equal); Software (equal); Supervision (equal); Writing – original draft (equal); Writing – review & editing (equal).

DATA AVAILABILITY

The data that support the findings of this study are available within the article and its supplementary material.

REFERENCES

[1] L. Zhu, M. Zhang, J. Xu, C. Li, J. Yan, G. Zhou, W. Zhong, T. Hao, J. Song, X. Xue *et al.*, "Single-junction organic solar cells with over 19% efficiency enabled by a refined double-fibril network morphology," Nat. Mater. **21**, 656–663 (2022).

[2] X.-H. Ma, J. Li, P. Luo, J.-H. Hu, Z. Han, X.-Y. Dong, G. Xie, and S.-Q. Zang, "Carbene-stabilized enantiopure heterometallic clusters featuring EQE of 20.8% in circularly-polarized OLED," Nat. Commun. **14**, 4121 (2023).

[3] Y. Yao, W. Huang, J. Chen, X. Liu, L. Bai, W. Chen, Y. Cheng, J. Ping, T. J. Marks, and A. Facchetti, "Flexible and stretchable organic electrochemical transistors for physiological sensing devices," Adv. Mater. **35**, 2209906 (2023).

[4] H. Lee, Z. Jiang, T. Yokota, K. Fukuda, S. Park, and T. Someya, "Stretchable organic optoelectronic devices: Design of materials, structures, and applications," Mater. Sci. Eng. R Rep. **146**, 100631 (2021).

[5] O. Ostroverkhova, "Organic optoelectronic materials: Mechanisms and applications," Chem. Rev. **116**, 13279 (2016).

[6] P. Yu, Y. Zhen, H. Dong, and W. Hu, "Crystal engineering of organic optoelectronic materials," Chem **5**, 2814 (2019).

[7] O. Sandberg, C. Kaiser, S. Zeiske *et al.*, "Mid-gap trap state-mediated dark current in organic photodiodes," Nat. Photon. **17**, 368 (2023).

[8] H. F. Haneef, A. M. Zeidell, and O. D. Jurchescu, "Charge carrier traps in organic semiconductors: A review on the underlying physics and impact on electronic devices," J. Mater. Chem. C **8**, 759 (2020).

[9] S. D. Baranovskii, "Mott lecture: Description of charge transport in disordered organic semiconductors: Analytical theories and computer simulations," Phys. Status Solidi A **215**, 1700676 (2018).

[10] C. Göhler, A. Wagenpfahl, and C. Deibel, "Nongeminate recombination in organic solar cells," Adv. Electron. Mater. **4**, 1700505 (2018).

[11] J. Mort, A. Troup, M. Morgan, S. Grammatica, J. C. Knights, and R. Lujan, "Geminate recombination in a-Si:H," Appl. Phys. Lett. **38**, 277–279 (1981).

[12] J. Kniepert, M. Schubert, J. C. Blakesley, and D. Neher, "Photogeneration and recombination in P3HT/PCBM solar cells probed by time-delayed collection field experiments," J. Phys. Chem. Lett. **2**, 700 (2011).

[13] Z. D. Popovic, "A study of carrier generation mechanism in x-metal-free phthalocyanine," J. Chem. Phys. **78**, 1552–1558 (1983).

[14] J. Kniepert, "Correlation between dynamic parameters and device performance of organic solar cells," Ph.D. thesis (Universität Potsdam, 2015).

[15] C. Wöpke, C. Göhler, M. Saladina, X. Du, L. Nian, C. Greve, C. Zhu, K. M. Yallum, Y. J. Hofstetter, D. Becker-Koch, N. Li, T. Heumüller, I. Milekhin, D. R. T. Zahn, C. J. Brabec, N. Banerji, Y. Vaynzof, E. M. Herzig, R. C. I. MacKenzie, and C. Deibel, "Traps and transport resistance: The next frontier for stable state-of-the-art non-fullerene acceptor solar cells," Nat. Commun. **13**, 3786 (2022).

[16] S. Shoaee, H. M. Luong, J. Song, Y. Zou, T.-Q. Nguyen, and D. Neher, "What we have learnt from PM6:Y6," Adv. Mater. **2023**, 2302005. doi:10.1002/adma.202302005.

[17] J. A. Röhr and R. C. I. MacKenzie, "Analytical description of mixed ohmic and space-charge-limited conduction in single-carrier devices," J. Appl. Phys. **128**, 165701 (2020).

[18] R. C. I. MacKenzie, C. G. Shuttle, M. L. Chabinyc, and J. Nelson, "Extracting microscopic device parameters from transient photocurrent measurements of P3HT:PCBM solar cells," Adv. Energy Mater. **2**, 662 (2012).

[19] R. MacKenzie, see http://oghma-nano.com for "Oghmanano" (2024).

[20] W. Shockley and W. T. Read, "Statistics of the recombinations of holes and electrons," Phys. Rev. **87**, 835–842 (1952).

[21] J. Kniepert and D. Neher, "Effect of the RC time on photocurrent transients and determination of charge carrier mobilities," J. Appl. Phys. **122**, 195501 (2017).

[22] J. Lorrmann, M. Ruf, D. Vocke, V. Dyakonov, and C. Deibel, "Distribution of charge carrier transport properties in organic semiconductors with Gaussian disorder," J. Appl. Phys. **115**, 183702 (2014).

[23] R. Hanfland, M. A. Fischer, W. Brütting, U. Würfel, and R. C. I. MacKenzie, "The physical meaning of charge extraction by linearly increasing voltage transients from organic solar cells," Appl. Phys. Lett. **103**, 063904 (2013).

[24] C. Göhler, A. Wagenpfahl, and C. Deibel, "Nongeminate recombination in organic solar cells," Adv. Electron. Mater. **4**, 1700505 (2018).

[25] J. Kniepert, A. Paulke, L. Perdigón-Toro, J. Kurpiers, H. Zhang, F. Gao, J. Yuan, Y. Zou, V. M. Le Corre, L. J. A. Koster, and D. Neher, "Reliability of charge carrier recombination data determined with charge extraction methods," J. Appl. Phys. **126**, 205501 (2019).

[26] J. Kurpiers and D. Neher, "Dispersive non-geminate recombination in an amorphous polymer:fullerene blend," Sci. Rep. **6**, 26832 (2016).

[27] J. Kniepert, I. Lange, N. J. van der Kaap, L. J. A. Koster, and D. Neher, "A conclusive view on charge generation, recombination, and extraction in as-prepared and annealed P3HT:PCBM blends: Combined experimental and simulation work," Adv. Energy Mater. **4**, 1301401 (2014).

[28] U. Würfel and M. Unmüssig, "Apparent field-dependence of the charge carrier generation in organic solar cells as a result of (bimolecular) recombination," Sol. RRL **2**, 1800229 (2018).

[29] A. Hofacker and D. Neher, "Dispersive and steady-state recombination in organic disordered semiconductors," Phys. Rev. B **96**, 245204 (2017).

14 May 2024 14:17:29